

# Observations of density fluctuations in an elongated Bose gas: ideal gas and quasi-condensate regimes

J. Esteve, J.-B. Trebbia, T. Schumm, A. Aspect, C. I. Westbrook, and I. Bouchoule  
*Laboratoire Charles Fabry, UMR 8501 du CNRS, 91 403 Orsay Cedex, France*

We report *in situ* measurements of density fluctuations in a quasi one dimensional  $^{87}\text{Rb}$  Bose gas at thermal equilibrium in an elongated harmonic trap. We observe an excess of fluctuations compared to the shot noise level expected for uncorrelated atoms. At low atomic density, the measured excess is in good agreement with the expected bunching for an ideal Bose gas. At high density, the measured fluctuations are strongly reduced compared to the ideal gas case. We attribute this reduction to repulsive interatomic interactions. The data are compared with a calculation for an interacting Bose gas in the quasi-condensate regime.

PACS numbers: 03.75.Hh, 05.30.Jp

The one dimensional (1D) Bose gas with repulsive interactions has attracted tremendous interest because of the rich behavior it exhibits as well as the existence of an exactly solvable model [1]. Recently, ultracold atoms have proven to be well adapted to testing theoretical predictions in various regimes. The transition towards the strong coupling regime, also called the Tonks-Girardeau regime has been observed [2, 3, 4, 5]. In the weak coupling regime, phase fluctuations of a quasi-condensate have been experimentally studied [6, 7, 8, 9, 10]. In this paper, we investigate spatial *density fluctuations* of a quasi 1D Bose gas in the weak coupling regime. The measurement relies on the analysis of noise in absorption images of atoms trapped on an atom chip. This technique was first proposed in Ref. [11], and used in Refs. [12] and [13] to observe atom-atom momentum correlations in other systems.

The weak coupling regime of a 1D Bose gas is characterized by  $\gamma = mg/\hbar^2 n \ll 1$  [14], where  $g$  is the effective 1D coupling constant,  $m$  is the atomic mass and  $n$  is the linear atom density. Within this regime, two limits can be distinguished depending on the temperature  $T$  of the sample compared to the temperature  $T_n$  defined by  $k_B T_n = \hbar n \sqrt{gn/m}$  [15, 16, 17]. For  $T \gg T_n$ , one recovers the ideal gas case. In this limit, density fluctuations are greater than would be expected for uncorrelated particles because of atom bunching [18, 19, 20]. Bunching refers to the enhanced probability of finding two identical bosons at the same place and arises from the exchange symmetry of their wavefunction. For  $T \ll T_n$ , the gas is in the so called Gross-Pitaevskii or quasi condensate regime. Repulsive interactions are important and density fluctuations are suppressed relative to the ideal gas case because of their energy cost. In this regime, phase fluctuations can be large as shown in [6, 7, 8, 9, 10]. A mean-field Bogoliubov approximation is valid and gives analytic predictions of the density and phase fluctuations.

Although our sample is not strictly 1D, our observations reflect these two regimes. At low density, we observe density fluctuations in excess of the atomic shot noise. This excess is in good agreement with the expected bunching for an ideal Bose gas. For high enough density, we observe a strong reduction of the fluctuations in qualitative agreement with the Bogoliubov approach.

Our measurements are conducted in a highly anisotropic magnetic trap created by an atom chip. We use three current carrying wires forming an H pattern [21] and an external uniform magnetic field to magnetically trap the  $^{87}\text{Rb}$  atoms in the  $|F = 2, m_F = 2\rangle$  state (see Fig. 1). Adjusting the currents in the wires and the external magnetic field, we can tune the longitudinal frequency between 7 and 20 Hz while keeping the transverse frequency  $\omega_\perp/(2\pi)$  at a value close to 2.85 kHz. Using evaporative cooling, we obtain a cold sample at thermal equilibrium in the trap. Temperatures as low as  $1.4 \hbar\omega_\perp/k_B$  are accessible with an atom number of  $5 \times 10^3$ . The atomic cloud has a typical length of  $100 \mu\text{m}$  along the  $z$  axis and a transverse radius of  $300 \text{ nm}$ .

As shown in Fig. 1, *in situ* absorption images are taken using a probe beam perpendicular to the  $z$  axis and reflecting on the chip surface at  $45^\circ$ . The light, resonant with the closed transition  $|F = 2\rangle \rightarrow |F' = 3\rangle$  of the D2 line is switched on for  $150 \mu\text{s}$  with an intensity of one tenth of the saturation intensity. Two images are recorded with a CCD camera whose pixel size  $\Delta \times \Delta$  in the object plane is  $6.0 \times 6.0 \mu\text{m}^2$ . The first image is taken while the trapping field is still on. The second image is used for normalization and is taken in the absence of atoms 200 ms later. During the first image, the cloud expands radially to about  $5 \mu\text{m}$  because of the heating due to photon scattering by the atoms. The size of the cloud's image is even larger due to resolution of the optical system (about  $10 \mu\text{m}$ ) and because the cloud and its image in the mirror at the atom chip surface are not resolved. Five pixels along the transverse direction  $x$  are needed to include 95% of the signal.

We denote by  $N_i^{\text{ph}}(x, z)$  the number of photons detected in the pixel at position  $(x, z)$  for the image  $i$  ( $i = 1, 2$ ). We need to convert this measurement into an atom number  $N(z)$  detected between  $z$  and  $z + \Delta$ . Normally, one simply computes an absorption per pixel  $\ln(N_2^{\text{ph}}/N_1^{\text{ph}})$  and sums over  $x$ :

$$N(z) = \sum_x \ln[N_2^{\text{ph}}(x, z)/N_1^{\text{ph}}(x, z)] \times \Delta^2/\sigma, \quad (1)$$

where  $\sigma$  is the absorption cross-section of a single atom. When the sample is optically thick and the atomic density varies on a scale smaller than the optical resolution

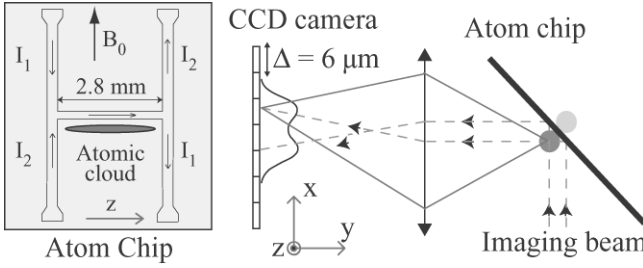


FIG. 1: Schematic of the experimental setup. Left: drawing of the wires constituting the atom chip. We keep  $I_1 + I_2 = 3 \text{ A}$  and adjust  $I_1 - I_2$  between 0.3 A and 1 A to vary the confinement along  $z$ . The uniform field  $B_0$  is approximately 40 G, we also add a small field ( $\lesssim 1 \text{ G}$ ) along  $z$ . Right: optical imaging system. We image the cloud and its reflection on the atom chip onto a CCD camera. In the radial direction, the unresolved cloud images cover approximately five pixels whose size in the object plane is  $\Delta = 6 \mu\text{m}$ .

or the pixel size, Eq. (1) does not hold since the logarithm cannot be linearized. In that case, Eq. (1) underestimates the atom number and the error increases with optical thickness. We partially correct for that effect by using in Eq. (1) an effective cross section  $\sigma$  determined as follows. We compare the measured atom number using the *in situ* procedure described above with the measured atom number after allowing the cloud to expand. In this case, Eq. (1) is valid and the atomic cross-section  $\sigma_0 = 3\lambda^2/(2\pi)$  well known. We then obtain for the effective cross-section  $\sigma = 0.8\sigma_0$ . Although this effective cross section depends on the atomic density, we have checked that for total atom number between  $2 \times 10^3$  and  $9 \times 10^3$  the measured value varies by only 10%. Taking into account the uncertainty on the value of  $\sigma_0$ , we estimate the total error on the measured atom number  $N(z)$  to be less than 20%.

To measure the variance of the atom number in a pixel, we acquire a large number of images (typically 300) taken in the same experimental conditions. To remove technical noise from our measurement, the following procedure is used to extract the variance. For each image, we form the quantity  $\delta^2 N(z) = (N(z) - \bar{N}(z))^2 \times p/(p-1)$  where the mean value  $\bar{N}(z)$  is normalized to contain the same total atom number as the current image. We thus correct for shot to shot total atom number fluctuations. The average is performed only over  $p = 21$  images which bracket the current image so that long term drifts of the experiment do not contribute to the variance. We have checked that the results are independent of  $p$ , varying  $p$  between 5 and 21. A large contribution to  $\delta^2 N(z)$ , irrelevant to our study, is the photon shot noise of the absorption measurement. To precisely correct for this noise, we subtract the quantity  $\sum_x (1/N_1^{\text{ph}}(x, z) + 1/N_2^{\text{ph}}(x, z))(\Delta^2\sigma)^2$  from  $\delta^2 N(z)$  for each image. We typically detect  $10^4$  photons per pixel corresponding to a contribution to  $\delta^2 N$  of about 50. To convert the camera signal into a detected photon number, we use a gain for each pixel that we determine by measuring the photon shot noise of images without atoms as explained in [22]. The corrected  $\delta^2 N(z)$  ob-

tained for all images are then binned according to the value of  $\bar{N}(z)$ , rather than of  $z$  itself. This gives the variance of the atom number  $\langle \delta^2 N(z) \rangle$  as a function of the mean atom number per pixel. Since more pixels have a small atom number, the statistical error on the estimate of the variance decreases with the average atom number (see Figs. (2) and (3)).

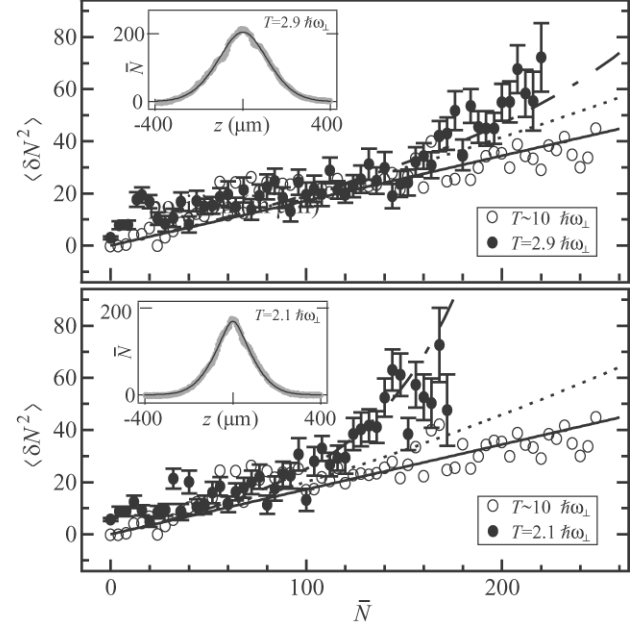


FIG. 2: Atom number variance as a function of the mean atom number per pixel. Open circles correspond to a "hot" cloud ( $T \simeq 10 \hbar \omega_{\perp}$ ,  $\omega_{\perp} = 2\pi \times 2.85 \text{ kHz}$ ) for which fluctuations are given by the shot noise (black line). The full circles correspond to cold clouds. The fluctuations in excess of shot noise are due to bosonic bunching. The dot-dashed line is the prediction for an ideal Bose gas while the dotted line uses the Maxwell-Boltzmann approximation (see Eq. (3)). The insets show the longitudinal profile of the two cold clouds from which we deduce the temperature and the chemical potential used for the calculations.

Data shown in Fig. 2 correspond to atom clouds of sufficiently low density so that interatomic interactions are expected to be negligible ( $T > T_n$ ). The three data sets correspond to three different temperatures, the trapping frequencies are 2.85 kHz and 7.5 Hz. We deduce the temperature and the chemical potential of the sample by fitting the mean longitudinal profile  $\bar{N}(z)$  of the cloud to the profile of an ideal Bose gas (see inset of Fig. 2). For the "hot" sample where bunching is negligible (see Eq. (3)), we observe atomic shot noise fluctuations, *i.e.* the atom number variance increases linearly with the mean atom number. The slope  $\kappa$  is only 0.17 and differs from the expected value of 1. We attribute this reduction to the fact that our pixel size is not much bigger than the resolution of our optical imaging system, thus one atom is spread out on more than one pixel. When the pixel size is small enough compared to the optical resolution and in the case of weak optical thickness, the expected slope is simply approximated by  $\kappa \simeq \Delta/(2\sqrt{\pi}\delta)$  where  $\delta$  is the rms width of the optical response that we suppose gaus-

sian. From the measured slope, we deduce  $\delta = 10 \mu\text{m}$  which is in good agreement with the smallest cloud image we have observed ( $8 \mu\text{m}$ ).

For "cold" samples, we see an excess in the atom number variance compared to shot noise. We attribute this excess to bunching due to the bosonic nature of the atoms. In a local density approximation, the fluctuations of a radially trapped and longitudinally uniform Bose gas with density  $n(z)$  are [20]

$$\langle n(z) n(z') \rangle - \langle n(z) \rangle^2 = \langle n(z) \rangle \delta(z - z') + \quad (2)$$

$$\frac{1}{\lambda_{\text{dB}}^2} \sum_{i,j \geq 1} \frac{e^{\beta\mu(i+j)}}{\sqrt{ij}} \frac{e^{-\pi(z-z')^2(\frac{1}{i}+\frac{1}{j})/\lambda_{\text{dB}}^2}}{[1 - e^{\beta\hbar\omega_{\perp}(i+j)}]^2}$$

where  $\mu$  is the local chemical potential,  $\beta = 1/(k_{\text{B}}T)$ ,  $\lambda_{\text{dB}} = \sqrt{2\pi\hbar^2/(mk_{\text{B}}T)}$  is the de Broglie thermal wavelength and  $\langle \cdot \rangle$  denotes an ensemble average. The first term on the right hand side corresponds to shot noise, and the second term to bunching. For a non degenerate gas ( $n\lambda_{\text{dB}} \ll 1$ ), one can keep only the term  $i = j = 1$ . The bunching term reduces to  $\langle n(z) \rangle^2 \exp(-2\pi(z-z')^2/\lambda_{\text{dB}}^2) \tanh^2(\beta\hbar\omega_{\perp}/2)$  and one recovers the well-known gaussian decay of the correlations as expected for a Maxwell-Boltzmann distribution. The reduction factor  $\tanh^2(\beta\hbar\omega_{\perp}/2)$  is due to the integration over the transverse states. In our experiment, the pixel size is always much bigger than the correlation length. In which case, integrating over the pixel size  $\Delta$ , we have

$$\langle N^2 \rangle - \langle N \rangle^2 = \langle N \rangle + \langle N \rangle^2 \frac{\lambda_{\text{dB}}}{\sqrt{2}\Delta} \tanh^2(\beta\hbar\omega_{\perp}/2). \quad (3)$$

The coefficient of  $\langle N \rangle^2$  is the inverse of the number of elementary phase space cells occupied by the  $N$  atoms. Because of the 1D geometry, the cell number is reduced and the bunching signal enhanced.

To compare Eq. (3) to our data we must correct for the optical resolution as was done for the shot noise. Furthermore, atoms diffuse about  $5 \mu\text{m}$  during the imaging pulse because of photon scattering. This diffusion modifies the correlation function, but since the diffusion distance is smaller than the resolution,  $10 \mu\text{m}$ , and since its effect is averaged over the duration of the pulse, its contribution is negligible. We thus simply multiply the computed atom number variance by the factor  $\kappa$ .

Figure 2 shows that the value calculated from Eq. (3) (dotted line) underestimates the observed atom number variance. In fact, for the coldest sample, we estimate  $n(0)\lambda_{\text{dB}} \simeq 10$ , and thus the gas is highly degenerate. In this situation replacing the Bose-Einstein occupation numbers by their Maxwell-Boltzmann approximations is not valid, meaning that many terms of the sum in Eq. (2) have to be taken into account. The prediction from the entire sum is shown as a dot-dashed line and is in better agreement with the data.

In the experiment we are also able to access a regime in which interparticle interactions are not negligible, and the ideal gas theory discussed above fails. Figure 3 shows the results of two experimental runs using colder and denser clouds of atoms. For these data, the trapping frequencies are 2.85 kHz and 10.5 Hz. The insets show the

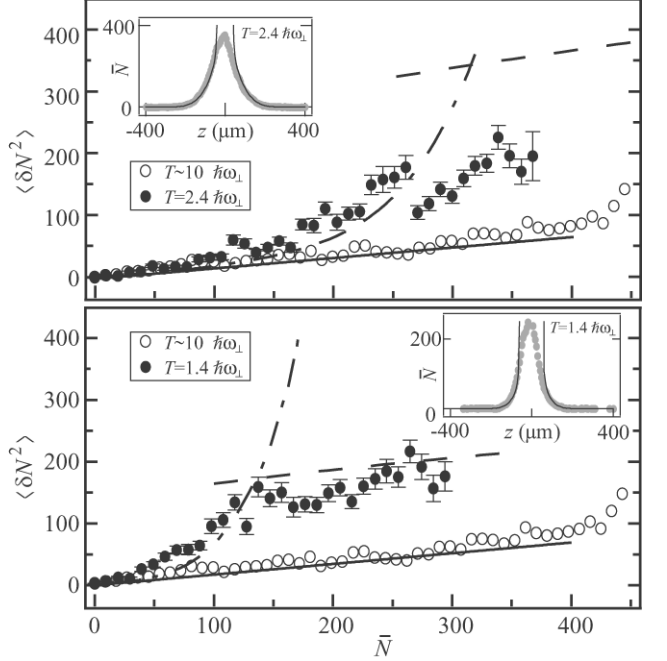


FIG. 3: We plot the same quantities as in figure 2. Dot-dashed lines are the predictions for an ideal Bose gas, whereas the dashed lines show the results of a calculation for a quasi-condensate in the Bogoliubov approximation (see Eq. 3). The temperature of the sample is deduced by fitting the wings of the longitudinal profile to an ideal Bose gas profile as shown in the insets.

mean longitudinal cloud profiles and a fit to the wings of the profiles to an ideal Bose gas profile. One can see from these insets that, unlike the conditions of Fig. 2, an ideal gas model does not describe the density profile in the center. We employ the same procedure to determine the variance versus the mean atom number. As in Fig. 2 we plot our experimental results along with the ideal Bose gas prediction based on the temperature determined from the fit to the wings in the insets. For small mean value  $\bar{N}(z)$ , the measured fluctuations follow the ideal gas curve (dot-dashed line) but they are dramatically reduced when the atom number is large.

The theory for a weakly interacting uniform 1D Bose gas permits an analytical prediction for the density fluctuations in the limit  $T \ll T_n$ . In this limit, the gas enters the Gross-Pitaevskii regime and density fluctuations are given in the Bogoliubov approximation by [15, 16]

$$\langle \delta n(z) \delta n(z') \rangle = \quad (4)$$

$$\frac{\langle n \rangle}{2\pi} \int_{-\infty}^{\infty} dk e^{ik(z-z')} \left( \frac{k^2}{k^2 + 4\xi^{-2}} \right)^{1/2} (1 + 2n_k),$$

where  $n_k$  is the Bose thermal occupation factor of the mode  $k$  with energy  $\epsilon_k = \sqrt{k^2(k^2 + 4\xi^{-2})} \times \hbar^2/(2m)$  and  $\xi = \hbar/\sqrt{mn\bar{g}}$  is the healing length. The term proportional to  $n_k$  describes the contribution of thermal fluctuations while the other is due to vacuum fluctuations and corresponds to the shot noise in the non interacting limit. Since the pixel size is much bigger than the healing length, we probe only long wavelength fluctuations

for which thermal fluctuations dominate at the temperatures we consider. Using  $k \ll 1/\xi$  and  $n_k \simeq k_B T/\epsilon_k$ , we obtain for the atom number variance in a pixel

$$\langle N^2 \rangle - \langle N \rangle^2 = \Delta \frac{k_B T}{g}. \quad (5)$$

This formula can also be deduced from thermodynamic considerations. The atom number variance is  $k_B T (\partial N / \partial \mu)_T$  which coincides with Eq. (5) for a gas with chemical potential  $gn$ .

To apply the previous calculation to our system, the effective 1D coupling constant  $g$  has to be computed. As long as  $n \ll 1/a$ , where  $a$  is the scattering length of the atomic interaction, the transverse profile of the cloud is given by the vibrational transverse ground state and  $g = 2\hbar\omega_\perp a$ , provided  $a \ll \sqrt{\hbar/(m\omega_\perp)}$ . For our experimental parameters,  $na$  can be as large as 0.7 and the transverse profile of the cloud is widened by interactions. To take this effect into account we make a gaussian ansatz for the profile and minimize the Gross-Pitaevskii energy functional. We then obtain  $g = 2\hbar\omega_\perp a / \sqrt{1 + 4na}$  as in [23]. Using this expression, we have computed atom number variance according to Eq. (4). The results are plotted in Fig. 3. The coupling  $g$  is not constant over the density range of interest and this explains the slope of the dashed line in Fig. 3.

The 1D calculation shown here relies on two assumptions. First, the higher branches of the Bogoliubov spectrum corresponding to transverse excitations are neglected and second the transverse shape of the relevant Bogoliubov modes is assumed to be identical to that of the Gross-Pitaevskii mode. A full 3D calculation shows that these assumptions are justified. From Fig. 3 we see that the calculation agrees well with the data for

$T = 1.4\hbar\omega_\perp$  but less so for  $T = 2.4\hbar\omega_\perp$ . Strictly speaking, the Bogoliubov approximation is valid in the limit  $T \ll T_n$  which corresponds to  $\langle N \rangle \gg 160$  (230) for  $T = 1.4\hbar\omega_\perp$  ( $T = 2.4\hbar\omega_\perp$ ). So apparently we did not achieve high enough density to reach the quasi-condensate regime for  $T = 2.4\hbar\omega_\perp$ .

A crucial aspect of this experiment has been the exploitation of the 1D geometry to avoid averaging the fluctuations in the imaging direction. This method can be applied to other 1D situations such as a Bose gas in the strong coupling regime, or an elongated Fermi gas, where sub shot noise fluctuations due to anti-bunching are expected. With increased optical resolution, one could also use this technique to measure the decay length of the density correlation function.

In the context of the 1D interacting Bose gas, our experiment raises the question of the nature of the transition towards the quasi-condensate regime in a very elongated trap. For a truly 1D Bose gas, in the thermodynamic limit, no phase transition is expected and the gas smoothly enters the quasi-condensate regime when the temperature is lowered [14]. This smooth transition may be masked in a finite size sample because of the saturation of the excited states, producing a more abrupt transition [24]. With our experimental parameters, a detailed study of these effects is possible.

This work has been supported by the EU under grants IST-2001-38863 and MRTN-CT-2003-505032, the DGA (03.34033), the ESF, and the "AC nano" program of the French research ministry. We thank D. Mailly from the Laboratoire de Photonique et Nanostructure (Marcoussis, France) for helping us to micro-fabricate the atom chip.

---

[1] E. H. Lieb and W. Liniger, Phys. Review **130**, 1605 (1963).  
[2] B. L. Tolra *et al.*, Phys. Rev. Lett. **92**, 190401 (2004).  
[3] B. Paredes *et al.*, Nature **429**, 277 (2004).  
[4] T. Kinoshita, T. Wenger, and D. Weiss, Science **305**, 1125 (2004).  
[5] H. Moritz, T. Stöferle, M. Köhl, and T. Esslinger, Phys. Rev. Lett. **91**, 250402 (2003).  
[6] S. Dettmer *et al.*, Phys. Rev. Lett. **87**, 160406 (2001).  
[7] S. Richard *et al.*, Phys. Rev. Lett. **91**, 010405 (2003).  
[8] D. Hellweg *et al.*, Phys. Rev. Lett. **91**, 010406 (2003).  
[9] M. Hugbart *et al.*, Eur. Phys. J. D. **35**, 155 (2005).  
[10] I. Shvarchuck *et al.*, Phys. Rev. Lett. **89**, 270404 (2002).  
[11] E. Altman, E. Demler, and M. D. Lukin, Phys. Rev. A **70**, 013603 (2004).  
[12] S. Fölling *et al.*, Nature **434**, 481 (2005).  
[13] M. Greiner, C. A. Regal, J. T. Stewart, and D. S. Jin, Phys. Rev. Lett. **94**, 110401 (2005).  
[14] D. S. Petrov, G. V. Shlyapnikov, and J. T. M. Walraven, Phys. Rev. Lett. **85**, 3745 (2000), and references therein.  
[15] C. Mora and Y. Castin, Phys. Rev. A **67**, 053615 (2003).  
[16] K. V. Kheruntsyan, D. M. Gangardt, P. D. Drummond, and G. V. Shlyapnikov, Phys. Rev. Lett. **91**, 040403 (2003).  
[17] Ü. Al Khawaja, J. O. Andersen, N. P. Proukakis, and H. T. C. Stoof, Phys. Rev. A **66**, 013615 (2002).  
[18] M. Yasuda and F. Shimizu, Phys. Rev. Lett. **77**, 3090 (1996).  
[19] M. Schellekens *et al.*, Science, published online in Science Express 15 September 2005 [DOI: 10.1126/science.1118024].  
[20] M. Naraschewski and R. J. Glauber, Phys. Rev. A **59**, 004595 (1999).  
[21] J. Reichel, Appl. Phys. B **75**, 469 (2002).  
[22] Y. Jiang *et al.*, Eur. Phys. J. D **22**, 521 (2003).  
[23] F. Gerbier, Europhys. Lett. **66**, 771 (2004).  
[24] N. J. van Druten and W. Ketterle, Phys. Rev. Lett. **79**, 549 (1997).